Annals of the BMVA Vol. 2012, No. ?, pp 1–? (2012)

Hierarchy in Anatomical Brain Networks Derived from Diffusion Weighted Images in 64 and 15 Directions

Fani Deligianni[1], Emma Claire Robinson[1], A. David Edwards[2], Daniel Rueckert[1], David Sharp[2], Daniel Alexander[4]
[1] BioMedIA group, Department of Computing, Imperial College London, UK
[2] Institute of Clinical Sciences, Imperial College and MRC Clinical Sciences Centre, Hammersmith Hospital, London, UK
[3] C3NL, Department of Medicine, Imperial College London, UK
[4] CMIC, Department of Computing, UCL, UK
Corresponding author: <fani.deligianni@imperial.ac.uk>

Abstract

Whole-brain structural connectivity matrices extracted from Diffusion Weighted Images (DWI) is a systematic way of representing anatomical brain networks. They are equivalent to weighted graphs that encode both the topology of the network as well as the strength of connection between each pair of regions of interest (ROIs). These matrices contain a significant amount of information for each subject that remains unexplored. In this work, we investigate whether connectivity matrices derived from ROIs with atlas-based parcellation and further sub-parcellations exhibit hierarchical organization. Furthermore, we exploit this topological property to enhance the classification performance in age and gender paradigms. Our results suggest that in DWI of 64-directions hierarchical organization can be exploited to improve classification. However, hierarchical organization in structural brain networks is confounded by atlas-based ROIs with uneven volumes. The low angular resolution of DWI in 15 non-collinear directions can also limit the ability to detect hierarchy in structural networks. Nevertheless, our results show that the topology of these brain networks encodes adequate information to characterize the age and gender of each subject. In our results, both gender

Annals of the BMVA Vol. 2012, No. ?, pp 1–? (2012)

and age classification relays on the topology of the network, whereas connectional strength has a minor role.

Keywords: brain connectivity, hierarchical organization, age classification, gender classification, brain network organization.

1 Introduction

Disruption in cortical connectivity has been implicated in a number of disorders and pathologies, such as schizophrenia [Burns, 2004], ADHD [Konrad and Eickhoff, 2010], autism [Müller, 2007], brain trauma [Kou et al., 2010, Pollonini et al., 2010] and so on. As a result there is a shift of research attention from localised brain abnormalities to dysfunction in network organization. Therefore, the investigation of structural brain connectivity, network topology and dynamics have become critical.

Anatomical brain connectivity refers to the existence of axonal connections between two brain areas. In non-human primates, it has been investigated extensively with the use of invasive tracing [Modha and Singh, 2010]. Typically, the extracted networks consist of regions located in gray matter that are hierarchically organized via axonal connections through white matter. Gray matter mostly consists of neuronal cell bodies, whereas white matter contains myelinated axons. This organization results in a small world topology with highly interconnected hubs and modularity both in a cellular and neuroimaging scale. With the advent of Diffusion Tensor Imaging (DTI), information regarding local connectivity is obtained non-invasively. Reconstructing and quantifying neuronal pathways based on this information remains a considerable challenge.

Diffusion Weighted MR Images (DWI) measure the mobility of brain water molecules *in vivo* [Beaulieu, 2002, Le Bihan et al., 2001]. Most MR visible water is enclosed within neuronal axons. With DWI diffusion anisotropy effects can be fully extracted and characterized, providing useful information about tissue microstructure. Structures such as myelin sheaths, axonal membranes, and micro-filaments cause the water diffusion to be slower perpendicular to axons than parallel to them. Within tissue with an oriented structure, such as white matter, the diffusion of water is higher in the direction of the fiber tracts. This directional dependence of water diffusion is called diffusion anisotropy. Diffusion anisotropy is thought to be partially correlated with barriers presented by axonal membranes and nerve myelination. Diffusion Tensor Imaging (DTI) exploits this property to estimate a vector field that represents the direction and the strength of anisotropy in each voxel.

There is an inherent complexity of connecting this directional information of each voxel and reproducing the neuronal pathways. These limitations originate from the fact that DTI is a macroscopic technique utilised to infer microscopic tissue properties. Furthermore, tracking accuracy may be affected by the background noise and partial volume effects in the raw images. Currently, there are several techniques to reconstruct fiber tracts [Behrens et al., 2003b, Mori and van Zijl, 2002]. Among the most successful is

Annals of the BMVA Vol. 2012, No. ?, pp 1–? (2012)

probabilistic tractography, which utilises a probabilistic framework to propagate local probability density functions on parameters in the diffusion model. Unlike other techniques, probabilistic tractography has been successfully used to extend fiber tracking even in gray matter [Behrens et al., 2003a, Lazar and Alexander, 2005, Parker and Haroon, 2003].

In probabilistic tractography a number of connections emerge that may or may not represent real fibers. It is important to understand that in a probabilistic framework, such as FSL [Behrens et al., 2003b], it is not straightforward to interpret probability. This is because it does not depend only on the likelihood of two brain areas to be connected but also on the uncertainty in the DWI data as well as the volume of the underlying ROIs [Robinson et al., 2008, Robinson et al., 2010]. Therefore, distance between ROIs and noise affects its values and prohibits comparisons across subjects and different populations. Recent techniques have been developed to model whole-brain connectivity and to assign a connectional strength between two brain regions based on measurements of diffusion anisotropy [Iturria-Medina and Canales-Rodriguez, 2007, Robinson et al., 2008].

Whole-brain structural networks carry a vast amount of information that it is hugely unexplored. Robinson et al. demonstrated that age classification can be performed with high accuracy based on whole-brain structural networks derived from diffusion tensor images [Robinson et al., 2010]. Their results are indicative of how informative whole-brain networks are about an individual. In their approach, they used a combined 83 ROIs atlas-based segmentation and soft-tissue segmentation to extract gray matter ROIs. Probabilistic tractography was employed to identify the tracts that connect each pair of regions. Connectivity was characterized based on localized measures of fractional anisotropy, which has been shown to be an indicator of fiber integrity and packing. Therefore, the regions' size has limited influence on connectivity characterization compared to probability measures. Gong et al. explored age and gender differences on the structural connectivity patterns derived from DWI [Gong et al., 2009]. Changes in the degree of local and global efficiency have been identified in anatomical networks derived based on a 78 ROIs cortical parcellation and probabilistic tractography.

Here we are interested in the hierarchical organization of these networks. Anatomical brain networks exhibit hierarchical organization starting from global systems of networks and ending in columnar subdivisions within these areas [Bullmore and Sporns, 2009, Golland et al., 2008, Salvador et al., 2005]. However, it is unclear whether this organization is maintained under different parcellations and scales in neuro-imaging studies. Zalesky et al. demonstrated that scale in brain networks can have a significant effect on their topological properties, such as small world, clustering and so on [Zalesky et al., 2010]. Furthermore, in probabilistic tractography a number of connections emerge that may or may not represent real fibers. Can we exploit the hierarchical organization of brain networks to redefine and eventually refine whole-brain connectivity matrices?

We propose inferring hierarchical structures from the observed anatomical connectivity with a technique that has been developed recently and has been tested in both biological and social networks [Clauset et al., 2008]. This technique uses statistical inference with Markov Chain Monte Carlo (MCMC) sampling algorithm to derive

Annals of the BMVA Vol. 2012, No. ?, pp 1–? (2012)

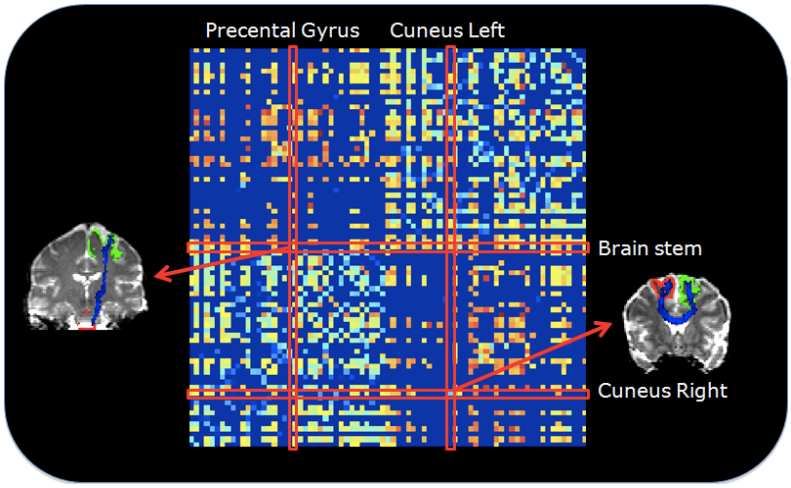

Figure 1: Whole-brain connectivity matrix for a subject. It has been extracted from a subject based on DWI in 64 directions and Robinson et al. methodology in estimating connectivity strength [Robinson et al., 2010]. This shows direct structural connections between each pair of cortical regions. The colormap reflects the strength of each connection with deep blue representing the absence of a structural connection between two regions. Regions of interest (ROIs) are plotted by cerebral hemispheres, with right-hemispheric ROIs in the lower left quadrant, left-hemispheric ROIs in the top right quadrant, and inter-hemispheric connections in the upper left and lower right quadrants.

hierarchical models, also called dendrograms, with probability proportional to the likelihood that they generate the observed network. Based on this approach a consensus dendrogram can be build that contains only the dendrogram's features that appear in the majority of the sampled models. This model allows the assignment of a probability for each connection that reflects the confidence in its existence based on the whole-brain network topology and the assumption that it is hierarchically organized. Spurious as well as missing connections can be identified based on their probability.

We use this methodology to analyze whole-brain connectivity matrices derived from a number of different sub-parcellations. A sub-parcellation strategy has been developed to subdivide each atlas-based ROI in sub-regions surrounded by a relatively equal portion of white matter voxels and an indicative number of voxels per area. We assume that improvement in the classification performance when whole-brain connectivity matrices are derived based on the MCMC algorithm reflects the hierarchical organization of the underlying network. We apply our approach in two paradigms of age (DWI in 15-directions) and gender (DWI in 15-directions and 64-directions) classification and we compare the performance of classification with and without the application of the hierarchical algorithm.

Annals of the BMVA Vol. 2012, No. ?, pp 1–? (2012)

2 Materials and Methods

2.1 Whole-brain connectivity - Overview

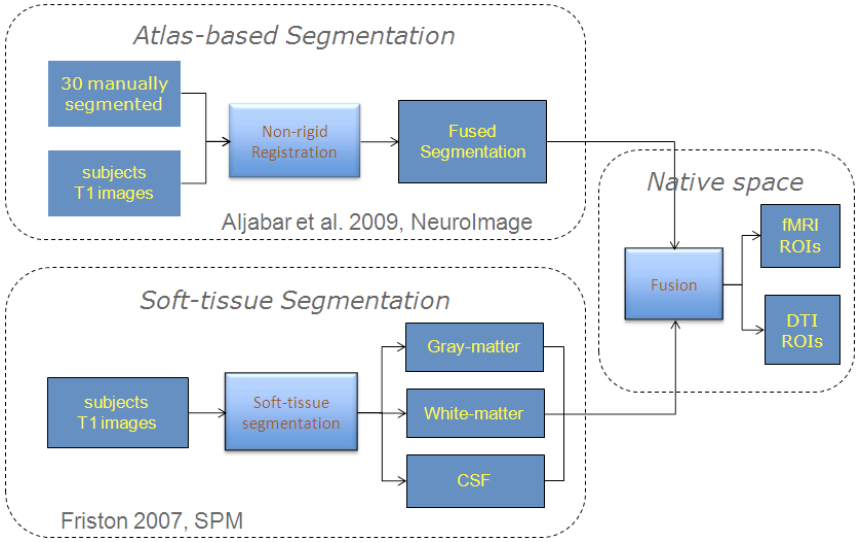

Figure 2: The combination of atlas-based segmentation and soft-tissue segmentation allows the delineation of anatomically sensible ROIs in gray matter. Atlas-based segmentation is based on established work [Aljabar et al., 2009], where 30 manually segmentations are propagated to the new subjects by non-rigid registration. SPM has been used for soft-tissue segmentation [J. Friston, 2007].

A structural connectivity matrix is a compact and systematic way to represent a brain network. In Figure 1, we show an example of a connectivity matrix extracted from a subject based on DWI in 64 directions and Robinson et al. methodology in estimating connectivity strength [Robinson et al., 2010]. This shows direct structural connections between each pair of cortical regions. Regions of interest (ROIs) are plotted by cerebral hemispheres, with right-hemispheric ROIs in the lower left quadrant, left-hemispheric ROIs in the top right quadrant, and inter-hemispheric connections in the upper left and lower right quadrants. The exact permutation of the ROIs follows established work in literature [Hagmann et al., 2008].

In this section, we provide an overview of how we extract whole-brain connectivity matrices from DWI. Firstly, we preprocess the DWI as well as the structural T1 images for each subject. This is followed by defining ROIs based on an 83-ROIs atlas-based segmentation, combined with soft-tissue segmentation. Based on these 83 ROIs a number of sub-parcellations can be obtained by subdividing each of these regions in sub-regions with equal number of voxels. Finally, an adapted framework of probabilistic tractography is employed to recover tracts between each pair of region and assign a weight that characterizes the strength of the connection.

Annals of the BMVA Vol. 2012, No. ?, pp 1–? (2012)

2.2 Preprocessing

FSL was the main tool for image pre-processing of DWI [Smith et al., 2004]. This involved eddy current correction of DWI and brain extraction. Brain extraction was manually refined later. Bias correction was applied to T1 and B0 images to improve the robustness of the non-rigid registration tools [Rueckert et al., 1999]. Intra-subject registration is usually accurate since both T1 and B0 have the exact same anatomy. However, we found that non-homogeneities of the 3T magnetic field can cause severe intensity bias in both T1s and B0s, which results in higher registration errors. For this reason we used bias correction for both T1s [Friston, 2007] and B0s [Sled et al., 1998]. The application of non-rigid registration is a major advantage of our methodology. Inter-subject label correspondence relies on accurate estimation of brain regions in diffusion space. Furthermore, fiber tracking is more reliable in white matter than gray matter. Therefore, it is critical to achieve highly accurate intra-subject registration between T1 and diffusion space (B0) that guarantees gray/white matter correspondence. Due to the 3T spatial distortions of diffusion imaging, affine registration is inadequate. Bias correction removed instabilities in the registration performance and allowed highly accurate and fully automated registration. We verified that the automatic atlas-based segmentation and transformation to native space was successful for all subject.

2.3 Brain Graphs Construction

Brain network construction was based on the fusion of atlas based segmentation and soft-tissue segmentation Figure 2. This facilitated the extraction of atlas-based ROIs that are located in gray-matter. Firstly, label propagation based on multiple atlases was used to segment each T1 image into 83 cortical and sub-cortical regions [Aljabar et al., 2009, Heckemann et al., 2006]. This is a highly accurate, automated approach that uses non-rigid registration [Rueckert et al., 1999] to propagate segmentation from 30 manually segmented images to new individuals. We utilized a state-of-the-art segmentation that selects the manual segmented images with the highest similarity to the new subject in order to achieve the best possible sub-folds/gyrus correspondence [Aljabar et al., 2007]. Atlas-based segmentation approaches are based on anatomical landmarks and they do not explicitly guarantee consistent underlying connectivity. However, they have been extensively used to define regions for the estimation of both structural and functional connectivity [Hagmann et al., 2008, Honey et al., 2009]. Compared to voxel-based approaches they do not require explicit inter-subject registration and they allow characterization of connectivity in native space. Recent work shows high reproducibility of structural connectivity matrices produced based on atlas-based segmentation [Cammoun et al., 2012]. Robustness has been demonstrated based on scanning data from the same subject as well as across subjects.

Neuronal activation is profound in gray matter, while DTI is more reliable in delineating white matter fibers [Koch et al., 2002]. Hence, probabilistic tissue segmentation was performed with SPM to classify gray matter, white matter and cerebrospinal fluid (CSF) [Friston, 2007]. Subsequently, atlas-based and tissue-based segmentation was fused

Annals of the BMVA Vol. 2012, No. ?, pp 1–? (2012)

to provide the final ROIs in native space. Segmentations were transformed to diffusion space with non-rigid registration [Rueckert et al., 1999].

2.4 Sub-Parcellation of ROIs

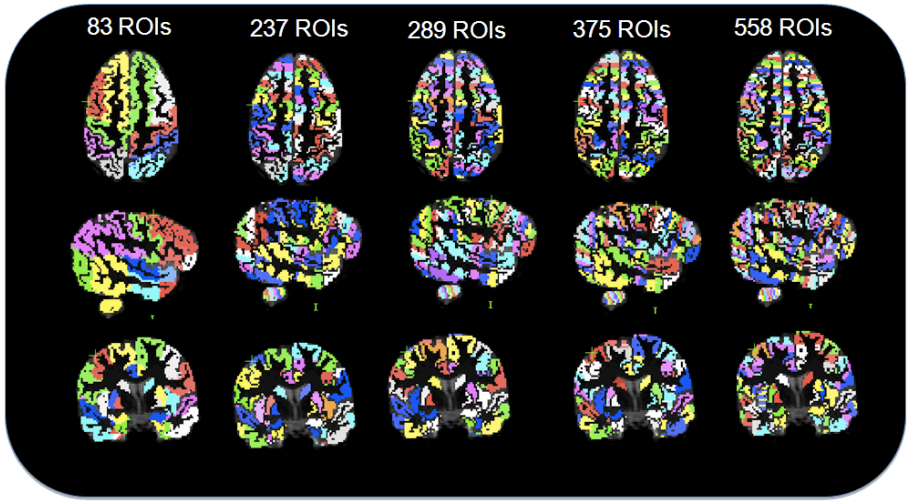

Figure 3: Axial, sagittal and coronal views of the original 83-ROIs parcellation as well as the four sub-parcellations in 243, 295, 381 and 564 ROIs. The sub-parcellations are produced based on the original 83-ROIs parcellation with the methodology that it has been described in details in section 2.4.

To sub-parcellate the 83 segmented ROIs, Figure 3, we transformed the segmentations from diffusion space into standard (MNI) space with affine registration. We counted the voxels within each region and across subjects and we predefined the number of sub-areas based on an indicative number of voxels per area. Each area was sub-divided in a number of regions, according to the average number of voxels across subjects divided by the indicative size and rounded to the closest integer. Subsequently, we extracted the boundary voxels of each ROI with white matter and we applied eigen-decomposition of the covariance matrix to define the plane that these points lay. The coordinates of each voxel in the ROI were projected on the first eigen-vector so that we could sub-divide them based on their projected position. Finally, they were subdivided into the predefined number of sub-regions so that each sub-region has equal number of voxels (±1). This way guarantees that all sub-regions within the original ROI are surrounded with relatively equal number of white matter voxels. Therefore, tracts between each sub-region and the rest ROIs can be identified.

2.5 Extraction of Structural Networks

Here, tracts between regions are identified using a standard probabilistic algorithm available as part of FSL [Behrens et al., 2003b, Smith et al., 2004]. However, we estimate the local diffusion anisotropy by determining the diffusive transfer between voxels using the orientation distribution function (ODF) [Iturria-Medina and Canales-Rodriguez, 2007, Robinson et al., 2010]. Note that the local diffusion anisotropy reflects changes in

myelination, fiber density and packing [Mädler et al., 2008]. For these reasons it has been used to quantify structural integrity in developmental, ageing and neurodegenerative studies [Kochunov et al., 2007, McKinstry et al., 2002, O'Sullivan et al., 2001]. In this framework, connectional strength can be compared across subjects and different populations.

2.6 From Brain Graphs to Hierarchical Random Graphs

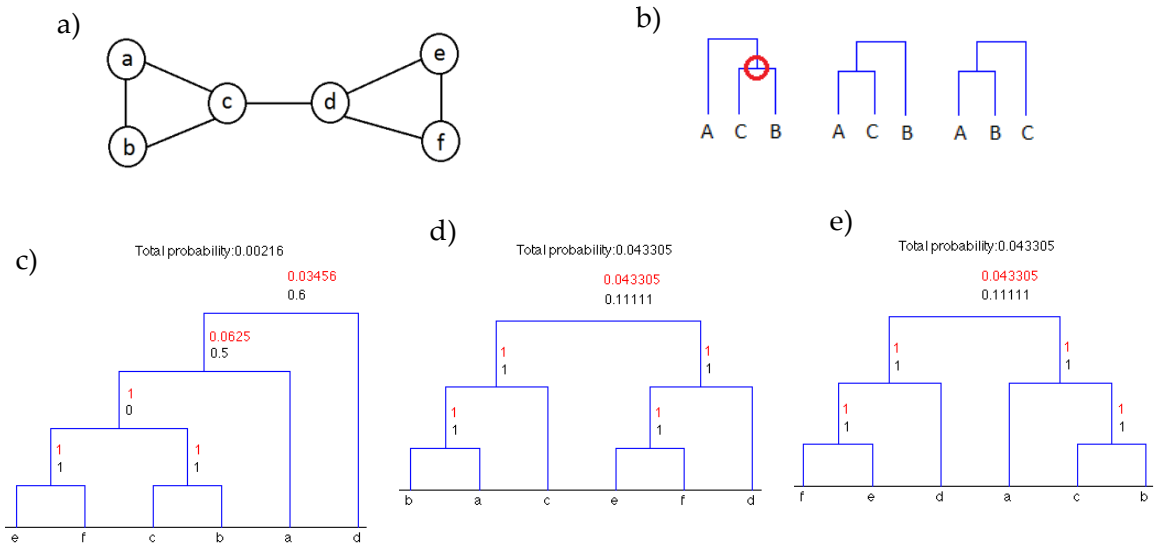

Figure 4: From graphs to dendrograms. a) An example graph with six nodes. b) Possible re-arrangements of a randomly chosen sub-tree during sampling. Once a random node is chosen (red circle), any of its children can exchange position with the parent node. c) A random dendrogram with leaves the nodes of the graph a) and five internal nodes. This can be the starting point of the MCMC algorithm. The numbers for each internal node of the dendrogram correspond to the probability $\overline{p_r}$ Eq. (1) and the intermediate terms in the product of Eq. (2) (black and red font respectively). d-e) Two examples of dendrograms that maximizes the likelihood Eq. (2) to represent the data in graph a). Note that re-arrangements of the nodes a,b,c or the nodes d,e,f within their sub-trees will not change the overall likelihood of the dendrogram.

In networks with hierarchical organization, nodes are subdivided into groups that are further subdivided into more groups and so forth over multiple scales. In brain networks, this implies that connections are dense within groups of areas and sparse between them. Clauset et al. showed that this property alone is able to explain both qualitatively and quantitatively a number of topological and statistical properties of the original graph, such as their degree distribution, clustering coefficient, distribution of shortest path lengths between pairs of vertices and so on [Clauset et al., 2008]. Their approach offers two major strengths: Firstly, it can capture both clusters of nodes, assortative, and disassociated nodes, disassortative structures, as well as arbitrary mixtures of the two, at all scales and parts of the network. Secondly, it does not depend on one hierarchical model but it

Annals of the BMVA Vol. 2012, No. ?, pp 1–? (2012)

generates a series of hierarchical models, dendrograms, and samples along them to create a consensus dendrogram that expresses the network's topology.

Let represent a structural brain network as a graph G with n nodes. The observed network data can be fitted to a random binary dendrogram based on a Monte Carlo sampling algorithm over a maximum-likelihood approach. A binary dendrogram has n leaves corresponding to the n nodes of the graph G, Figure 4a and each of the $n-1$ internal nodes has exactly two descendants, Figure 4(c-e). Each internal node r is associated with a probability p_r. Under a maximum-likelihood approach the probability p_r is estimated as the fraction of edges between the two sub-trees:

$$\overline{p_r} = \frac{E_r}{L_r R_r} \tag{1}$$

Where E_r are the edges between left and right sub-trees and L_r and R_r are the number of nodes in left and right sub-tree, respectively. The likelihood of the dendrogram at this maximum is given below:

$$L(D) = \prod_{r \in D} \left[\overline{p_r}^{\overline{p_r}} (1-\overline{p_r})^{1-\overline{p_r}}\right]^{L_r R_r} \tag{2}$$

The overall likelihood of the dendrogram reflects how well the dendrogram fits the graph data under the assumption that the original graph has hierarchical organization. Here we used the logarithm of the likelihood to avoid numerical instabilities due to very small numbers.

$$logL(D) = -\sum_{r \in D} L_r R_r h(\overline{p_r}) \tag{3}$$

Where h is the Gibbs-Shannon entropy function for a binary system: $h(p) = -plogp - (1-p)log(1-p)$. From this equation, we note that dendrogram with high probability are those that partition the vertices into groups that are either very well interconnected or disconnected.

Subsequently, the Markov Chain Monte Carlo (MCMC) method is used to sample dendrograms with probability proportional to their likelihood. In a Monte Carlo simulation, it is important to generate an appropriate random set of states according to Boltzmann probability distribution. A Markov process is the generating engine of this set. According to this process the probability from one state μ to another ν depends only on steps μ and ν. This Markov process should follow certain conditions. For example, it should be possible to reach any state of the system from any other. Here, the Markov chain consists of re-arrangements of subtrees of the dendrogram as shown in Figure 3b. An internal node r is chosen with a uniform random distribution. Subsequently, any of the two configurations can apply at random to transform the dendrogram to a new state. This state is accepted or rejected according to the Metropolis-Hasting rules. According to this a transition between two dendrograms $D \rightarrow \acute{D}$ is accepted either if the dendrogram $\acute{D}$ has higher likelihood than D or with probability equal to the ratio of their likelihoods:

$$exp(log\Delta\mathcal{L}) = \mathcal{L}(\acute{D})/\mathcal{L}(D) \quad (4)$$

These rules guarantee detailed balance, which implies that the system will reach equilibrium. Equilibrium is defined as the condition where the rate at which the system makes transitions into and out of any state must be equal. The condition of detailed balance also guarantees that the MCMC is not trapped into a limit cycle, in which the probability distribution rotates around a number of different values, dynamic equilibrium. MCMC is commonly used in the context of Bayesian statistics along with a uniform prior distribution. In our work, specification of a uniform prior distribution on the space of dendrograms is not necessary.

2.7 Construction of Probability Maps of Brain Connectivity

Once MCMC reaches equilibrium, dendrograms can be sampled at regular interval from the Markov chain. For each sampled dendrogram a probability connectivity matrix can be created with values that reflect the probability of each pair of nodes/areas to be connected. The probability between each pair of nodes i and j is equal to the probability $\overline{p_r}$ of the lowest common ancestor of the nodes i and j in the sampled dendrogram. A consensus probability matrix is estimated by averaging these matrices across dendrogram samples.

3 Results

We implemented the MCMC algorithm in MATLAB and tested our approach with DWI in 64 and 15 directions. In this section, we describe firstly our main methodology steps applied in 64 directions data for gender classification of 20 subjects. Subsequently, we used MCMC to create probability connectivity matrices and evaluate how informative they are in both age and gender classification paradigms of 90 subjects and DWI in 15 directions. Classification performed in a number of different parcellations with the application of the MCMC methodology and based on the original connectivity matrices alone.

3.1 64-Directions DWI Data: Gender Classification

We used diffusion weighted images (DWI) that have been acquired from 20 normal volunteers (10 males, 10 females) with the following imaging parameters: 64 non-collinear directions, in 72 slices, slice thickness 2 mm, FOV 224mm, matrix 128x128, voxel size 1.75x1.75x2mm^3, b value 1000 s/mm^2 (Philips 3Tesla).

In this paradigm, we aimed to explore whether different parcellation of the cortex would affect the efficiency of the hierarchical clustering and subsequently the overall classification rate. Based on the original 83-ROIs segmentation, we created four sub-parcellations with an indicative size of region of 500, 400, 300 and 200 voxels per area, Table 1. This resulted in four segmentations with 243, 295, 381 and 564 regions, respectively, Figure 3. We run the adapted probabilistic tractography [Robinson et al., 2010], which estimated the connectional strength between each pair of regions and

Annals of the BMVA Vol. 2012, No. ?, pp 1–? (2012)

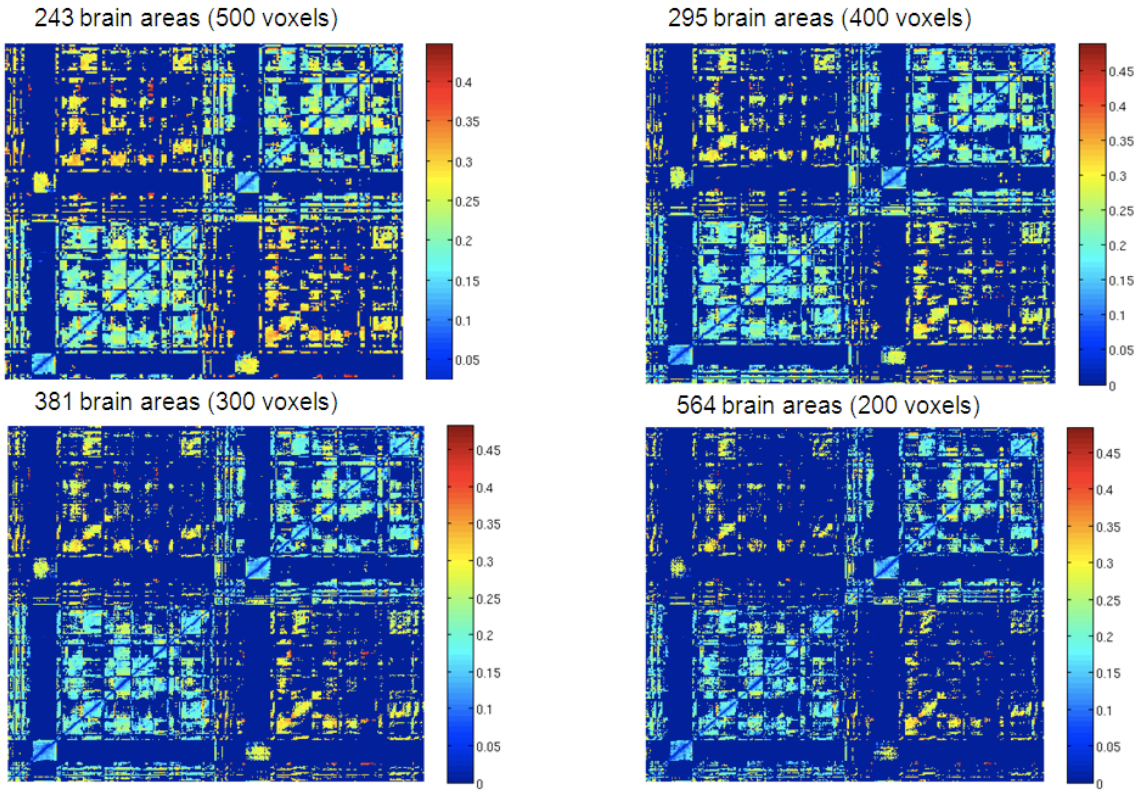

Figure 5: Structural connectivity matrices of the same subject that correspond to the sub-parcellations in Figure 4 and they are obtained based on the Robinson et al. methodology in estimating connectional strength [Robinson et al., 2010].

provided with the corresponding connectivity matrices for each sub-parcellation, Figure 5. It is apparent that each of these connectivity matrices exhibits hierarchical organization compared to the original parcellation, since the smaller areas within the larger original 83-ROIs are highly interconnected, Figure 5.

For each subject and each parcellation, we run the MCMC method till the algorithm reached equilibrium. The algorithm can reach its minimum, zero, only when there are no missing links in the graph and the graph is hierarchical. In other words, it consists of clusters of nodes that are fully interconnected or completely disconnected. Otherwise, it settles to an equilibrium state, during which it samples along dendrograms of similar likelihood. Once the MCMC has reach equilibrium, the probability that there is a connection between each pair of nodes, i and j, is estimated as the probability $\overline{p_r}$ of the lowest common ancestor that connects i and j. This probability is averaged across a predefined number of dendrogram (5000) in equilibrium stage. These new connectivity matrices depict the probability that two nodes are connected.

We performed gender classification by separating subjects into two groups according to their gender and averaging the mean-subject probability connectivity matrices [Deligianni et al., 2011]. We used leave-one-out cross validation to classify the subjects based on the normalised Euclidean distance between the average probability maps of each

group and the leave-one-out subject. If the subject's distance from the male group is higher than its distance from the female group, we classify the subject as female and vice-versa. To demonstrate the efficiency of our methodology we also performed classification with the original connectivity matrices and the same classifier [Robinson et al., 2010]. In Figure 6, the Receiver Operating Characteristic (ROC) curve is shown for each of the sub-parcellations with and without MCMC. The Area Under the Curve (AUC) is a measure of the optimum performance of the classifier. Our results suggest that age classification is not successful based on the original parcellation alone neither with the application of the MCMC algorithm (41% classification rate) or without (56% classification rate). However, when we analyzed the sub-parcelated connectivity matrices with the MCMC approach, we could classify the subjects with up to 82% classification rate. Gender classification based on the original connectivity matrices was unsuccessful for all the different sub-parcellation scenarios. Since MCMC has as input binary matrices (one when a connection exist, zero for the absence of connection), we also classified the binarised version of the original connectivity matrices. This would clarify whether classification performance is due to the original topology or the additional information of connectional strength. The results (not shown) are similar to Figure 6 (b).

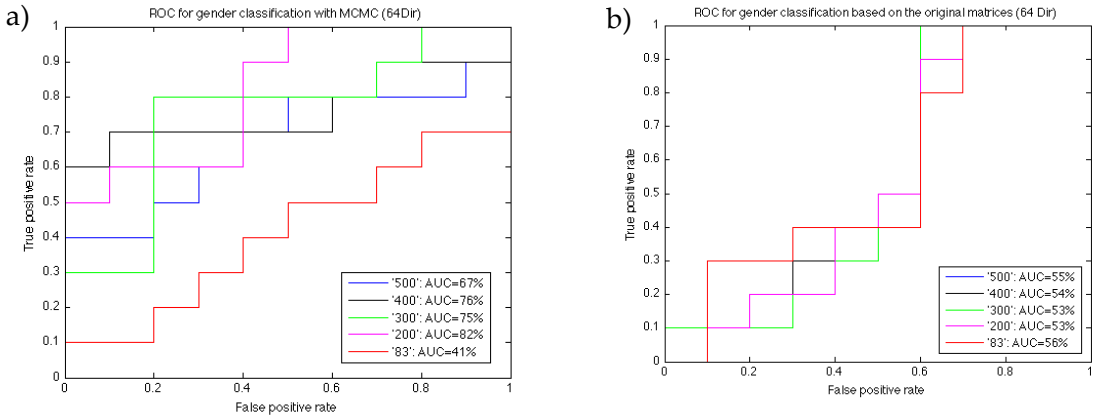

Figure 6: Receiver Operating Characteristic (ROC) curve is plot of the sensitivity versus 1-specificity for a binary classifier as its discrimination threshold is varied. Here the area under the curve (AUC) is a measure of the optimum performance of the classifier. a) ROC for gender classification with the MCMC methodology for each of the parcellations in Figure 3. b) ROC for gender classification based on the original connectivity matrices of each parcellation scenarios in Figure 3.

3.2 15-Directions DWI Data: Age and Gender Classification

We used data that are available publically under the IXI database: http://www.ixi.org.uk. The T1 and T2 images were acquired using 3D MRPRAGE and dual echo weighted imaging. We used DWI that have been acquired from 90 normal volunteers with the following imaging parameters: Single shot echo planar DTI in 15 non-collinear directions, TR 12,000msec, TE 51msec, slice thickness 2mm, voxel size 1.75x1.75x2mm^3 (Philips

Annals of the BMVA Vol. 2012, No. ?, pp 1–? (2012)

3Tesla). Analysis was performed on 90 adult healthy volunteers. In this section, we tried both age (41 young subjects, 20-30 years old, 49 old subjects, 60-90 years old) and gender (52 females, 38 males) classification.

We followed the methodology in section 3.1 with leave-one-out cross validation. In Table 2 are the number of sub-parcelated areas along with the mean, max and min number of voxels across all areas and subjects. Age and gender classification results are summarized in Figure 7, which shows the AUC results based on ROC curves. The age classification based on the original sub-parcelated connectivity matrices outperforms the results obtained from the 83-ROIs parcellation. Since MCMC has as input binary matrices (one when a connection exist, zero for the absence of connection), we also classified the binarised version of the original connectivity matrices. This would clarify whether classification performance is due to the original topology or the additional information of connectional strength. Gender classification performs well without any information about the fractional anisotropy along the tracts. For age classification is less clear whether connectional strength has the potential to improve classification.

Table 1: Sub-parcellation (64-Dir Data): number of sub- areas, mean-max-min of number of voxels in each area.

	Original Parcellation	500 voxels/area	400 voxels/area	300 voxels/area	200 voxels/area
numSubAreas	83	243	295	381	564
MeanNumVox	1424±1786	486±143	401±100	310±67	210±35
MaxNumVox	8135	814	608	490	318
MinNumVox	28	28	28	28	28

Table 2: Sub-parcellation (15-Dir Data): number of sub-areas, mean-max-min of number of voxels in each area.

	Original Parcellation	500 voxels/area	400 voxels/area	300 voxels/area	200 voxels/area
numSubAreas	83	194	239	299	438
MeanNumVox	1042±1250	446±153	362±102	289±70	197±35
MaxNumVox	5098	741	607	440	297
MinNumVox	21	21	21	21	21

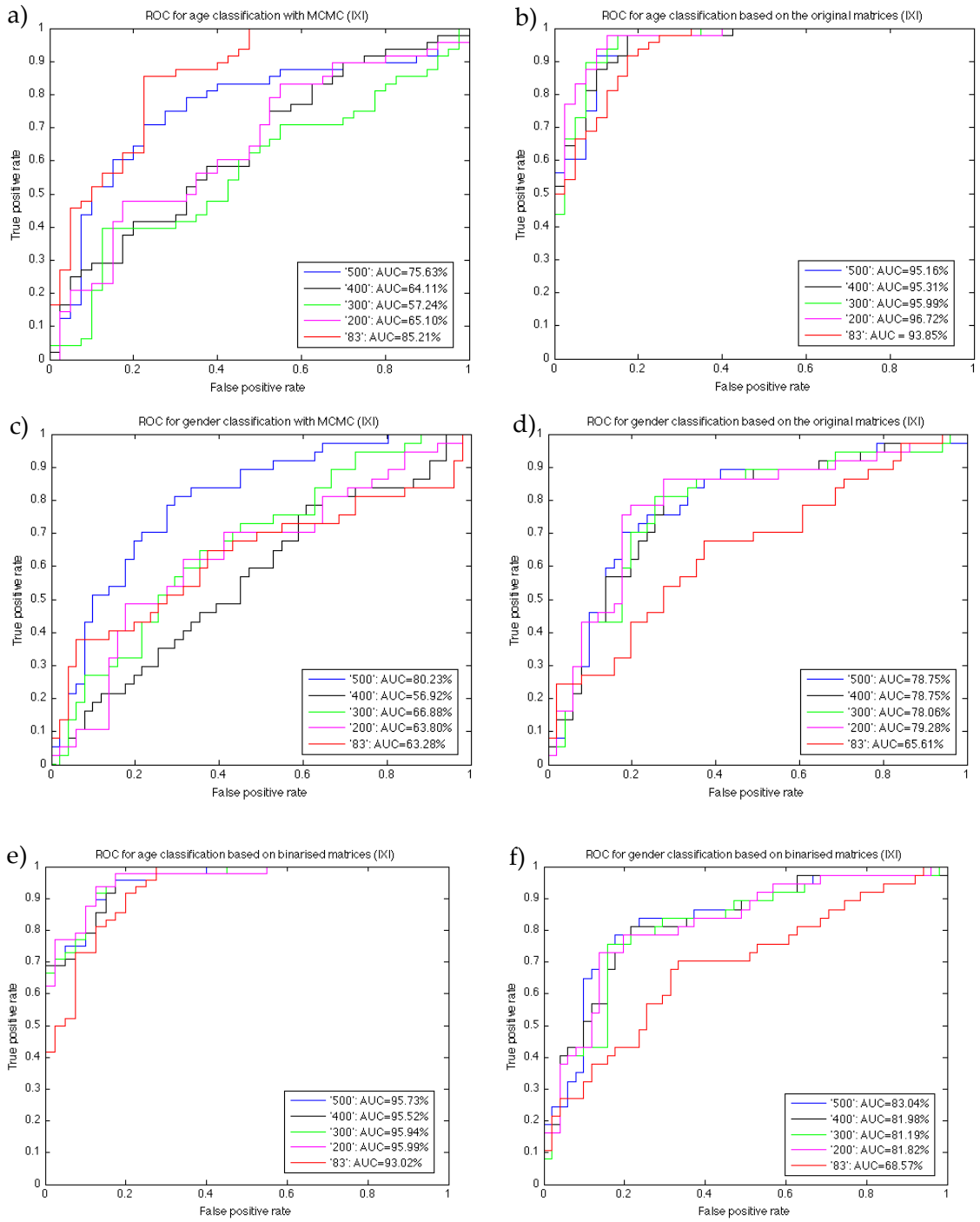

Figure 7: ROC curves for age classification (top row) and gender classification (bottom row) for each of the different subparcellation scenarios. a) ROC curves for age classification with the application of the MCMC methodology, b) ROC curves for age classification on the original matrices, c) ROC curves for gender classification with the application of the MCMC methodology. d) ROC curves for gender classification based on the original matrices, e) ROC curves for age classification based on the binarised connectivity matrices (0 if there is no connection and 1 if there is a connection), f) ROC curves for gender classification based on the binarised connectivity matrices.

Annals of the BMVA Vol. 2012, No. ?, pp 1–? (2012)

4 Discussion

Here we use a hierarchical algorithm (MCMC) [Clauset et al., 2008] to infer probability of connection between each pair of brain region based on the assumption that brain networks exhibit hierarchical organization. This approach is powerful in detecting missing links and false positives based only on the topology of the network. We were interested in testing how a variety of sub-parcellations and angular resolution of diffusion data can affect the age and gender classification performance with or without the application of MCMC. We hypothesized that enhancement of the classification performance is an indication that the underline network is hierarchically organized and the MCMC is able to improve its topology. We used a novel approach to sub-parcelate each from the original 83-ROIs in sub-regions that are surrounded with relatively equal number of white matter voxels. This sub-parcellation aimed to split gray matter in ROIs that have relatively equal number of voxels and also respect the boundaries between the original 83-ROIs atlas. In this way, we could investigate how hierarchy is expressed in different scales.

We applied our approach successfully in a gender classification paradigm of 20 subjects with diffusion data in 64 directions. Our results showed that although classification performance did not improve in the case of the original 83-region parcellation, it was significantly enhanced in all other sub-parcellations. This suggests that hierarchical organization of anatomical networks derived from DWI can be confounded by the uneven sub-parcellation in 83-regions with size that varies from 20 to over 8000 voxels. On the other hand, MCMC applied on connectivity matrices derived from the sub-parcellation has a significant improvement in classification over the original connectivity matrices. It is important to note that the MCMC started with binary matrices (one for a connection and zero for the absence of a connection) and thus operates based only on the topology of the network. The original connectivity matrices are more informative, since their weights are related to fractional anisotropy. However, the MCMC was capable of outperforming gender classification only based on the network's organization. This may suggest that gender differences are not only due to differences in the strength of the connections between different thalamo-cortical areas but they are also profound in the topology of the network.

Subtle differences between males and females have been also reported in the organization and microstructure of specific brain connections. Sex differences in the organization of the corpus callosum have been found and they may be linked to differences in functional lateralization between men and women [Oh et al., 2007]. A recent study has also confirmed these results with a combination of DTI and myelin-water fraction imaging [Liu et al., 2010]. Animal studies have been also demonstrated significantly greater oligodendrocyte density in the corpus callosum of male rodents, relative to females [Cerghet et al., 2009]. These results suggest that there are sex differences in the microstructural composition and organization of the inter-hemispheric tracts.

Gender classification in 90 subjects with diffusion data in 15 non-collinear directions did not performed better than directly classifying the original connectivity matrices, Figure 7. We argue that this is because of missing connections due to the limited angular

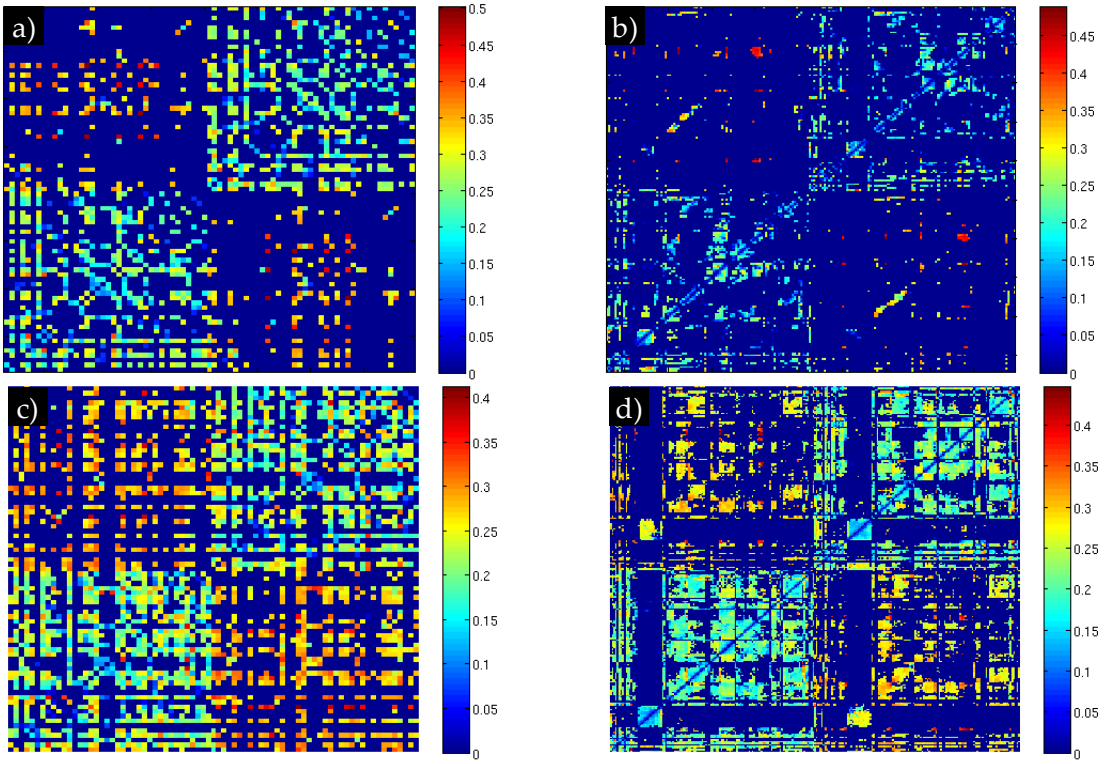

Figure 8: Connectivity matrices obtained based on: a) 83-ROIs anatomical atlas for the diffusion data in 15 non-collinear directions, b) '500' sub-parcellation for the same DWI data as a), c) 83-ROIs anatomical atlas for diffusion data in 64 non-collinear directions, d) '500' sub-parcellation for the same diffusion data c).

resolution of the diffusion data (15 non-collinear directions). For example, Figure 8 shows a typical example of connectivity matrices derived from diffusion data of 15 directions compared with connectivity matrices derived from diffusion data in 64 directions. Note that probabilistic tractography fails to recover a substantial number of inter-hemispheric connections. This problem is particularly profound in the sub-parcellations, which results in severally affecting the topology of the network. The inability to track inter-hemispheric connections may also explain why gender classification with MCMC is not particularly successful in the 15-directions dataset, since significant sex differences have been identified in inter-hemispheric connections [Cerghet et al., 2009]. It is encouraging though that the sub-parcellation improves the performance of classification with or without the application of MCMC.

We also used an age classification paradigm in order to be able to draw conclusions about how well our approach performs compared to results published in literature [Robinson et al., 2010]. It is widely accepted that ageing has profound effects in brain connectivity as well as diffusion anisotropy. There are several studies that show the effect of ageing in human anatomy and function [Esposito et al., 1999, Kochunov et al., 2007, O'Sullivan et al., 2001, Stark and Pakkenberg, 2004]. It has been shown that anisotropy within the white matter of the brain increases dramatically during early stages of

Annals of the BMVA Vol. 2012, No. ?, pp 1–? (2012)

development and myelination [McKinstry et al., 2002]. This continues throughout childhood [138] into early adulthood. Subsequently, it declines slowly till 50-60 years old and rapidly thereafter. Healthy ageing is also characterised by decreased white matter anisotropy between frontal and posterior regions of the brain [O'Sullivan et al., 2001]. Furthermore, decreased anisotropy in frontal white matter during ageing is correlated with reduced executive functions such as problem solving and working memory [O'Sullivan et al., 2001]. These demonstrate a link between white matter anisotropy and cognitive decline in normal ageing. Gender differences in literature have been more controversial than differences due to ageing, which may explain why gender classification performance is lower than age classification performance under all scenarios.

Evidence in current literature [Cammoun et al., 2012] show high reproducibility of structural connectivity matrices based on atlas-based segmentations and sub-parcellated versions. This indicates that even a simple Euclidean distance can capture differences in normal populations. Bernadette et al. notes that methods that compare networks based on topological measures, such as clustering coefficient and characteristic path length should account for the different size (number of nodes) and graph density (number of edges) [Wijk et al., 2010]. To alleviate this problem, we derive fully connected graphs from the MCMC algorithm that reflect probability of connection for each pair of regions. Note that the number of nodes is identical in each graph. Subsequently, we form a Euclidean measure that estimates the difference between each corresponding edge. This is a naïve measure of graph distance, which can be seen as an extension of Hamming distance in weighted graphs. This formulation can extend to address heteroscedastically-distributed connections and, subsequently, outliers, which are profound in population groups with pathology. Further work should investigate similarity measures between weighted connectivity graphs.

Analyzing weighted graphs constitute a tremendous challenge in current literature. Simply thresholding these networks results in topology, which is indeed intertwined with connectional strength [Ginestet et al., 2011]. It is important to note that, in our work, binarised structural networks are not derived using an arbitrary threshold. Instead, the absence of a connection reflects the lack of directional information to support a pathway between two regions. Therefore, it is an inherent topological property of the underlying imaging data.

5 Conclusions

Originally the MCMC model has been suggested for examining missing connections as well as false positive by inferring hierarchical structure from the observed anatomical connectivity [Clauset et al., 2008]. Here we showed that this approach has the potential to improve the topology of brain connectivity matrices. In fact, we examined whether whole-brain connectivity matrices exhibit hierarchical organization under different parcellations.

A gender and age classification paradigms were employed to explore how informative the underline brain network topology is with regard to the gender and age of each individual. Our results suggest that the connectivity matrices of the sub-parcelated ROIs, but not the original 83-ROIs segmentation, exhibit hierarchical organization. This organization can be exploited to improve classification in diffusion data in 64 non-collinear directions. However, the topology of networks derived from diffusion data in 15 non-collinear directions is corrupted to an extent that it cannot be fully recovered from the MCMC algorithm. Further work with a larger dataset of diffusion data in 64-directions data should be conducted to be able to confirm whether age classification can be improved with the application of our approach.

Acknowledgements

The authors are grateful for the support from MRC (G0701782) and NIHR Imperial College Comprehensive Biomedical Research Centre.

References

P. Aljabar, R. Heckemann and A. Hammers. Classifier selection strategies for label fusion using large atlas databases. *MICCAI*: 523-31, 2007.

P. Aljabar, R.A. Heckemann, A. Hammers, J.V. Hajnal and D. Rueckert. Multi-atlas based segmentation of brain images: atlas selection and its effect on accuracy. *NeuroImage,* 46: 726-38, 2009.

C. Beaulieu. The basis of anisotropic water diffusion in the nervous system: a technical review. *NMR Biomed.,* 15: 435-55, 2002.

T. Behrens, H. Johansen-Berg and M. Woolrich. Non-invasive mapping of connections between human thalamus and cortex using diffusion imaging. *Nat. Neurosci.,* 6: 750-57, 2003a.

T. Behrens, M. Woolrich, M. Jenkinson, H. Johansen-Berg, R. Nunes, S. Clare, P. Matthews, J. Brady and S. Smith. Characterization and propagation of uncertainty in diffusion-weighted MR imaging. *Magnet Reson Med,* 50: 1077-88, 2003b.

E. Bullmore and O. Sporns. Complex brain networks: graph theoretical analysis of structural and functional systems. *Nat. Rev. Neurosci.,* 10: 186-98, 2009.

J. Burns. An evolutionary theory of schizophrenia: Cortical connectivity, metarepresentation, and the social brain. *Behav. Brain Sci.,* 27: 831-55, 2004.

L. Cammoun, X. Gigandet, D. Meskaldji, J.P. Thiran, O. Sporns, K.Q. Do, P. Maeder, R. Meuli and P. Hagmann. Mapping the human connectome at multiple scales with diffusion spectrum MRI. *J. Neurosci. Methods,* 2032012.

M. Cerghet, R.P. Skoff, M. Swamydas and D. Bessert. Sexual dimorphism in the white matter of rodents. *J Neurol Sci,* 286: 76-80, 2009.

A. Clauset, C. Moore and M. Newman. Hierarchical structure and the prediction of missing links in networks. *Nature,* 453: 98-101, 2008.

Annals of the BMVA Vol. 2012, No. ?, pp 1–? (2012)

F. Deligianni, E. Robinson, D. Sharp, A.D. Edwards, D. Rueckert and D.C. Alexander. Hierarchy in structural brain networks. *MIUA*, 2011.

G. Esposito, B. Kirkby, J. Van Horn and T. Ellmore. Context-dependent, neural system-specific neurophysiological concomitants of ageing: mapping PET correlates during cognitive activation. *Brain*, 122: 963-79, 1999.

K. Friston. Statistical parametric mapping: the analysis of functional brain images. 647, 2007.

C.E. Ginestet, T.E. Nichols, E.T. Bullmore and A. Simmons. Brain Network Analysis: Separating Cost from Topology Using Cost-Integration. *PLoS ONE*, 6: e21570, 2011.

Y. Golland, P. Golland, S. Bentin and R. Malach. Data-driven clustering reveals a fundamental subdivision of the human cortex into two global systems. *Neuropsychologia*, 46: 540-53, 2008.

G. Gong, P. Rosa-Neto, F. Carbonell, Z.J. Chen, Y. He and A.C. Evans. Age- and Gender-Related Differences in the Cortical Anatomical Network. *J Neurosci*, 29: 15684-93, 2009.

P. Hagmann, L. Cammoun, X. Gigandet, R. Meuli, C.J. Honey, V.J. Wedeen and O. Sporns. Mapping the structural core of human cerebral cortex. *PLoS Biol*, 6: 1479-93, 2008.

R.A. Heckemann, J.V. Hajnal, P. Aljabar, D. Rueckert and A. Hammers. Automatic anatomical brain MRI segmentation combining label propagation and decision fusion. *NeuroImage*, 33: 115-26, 2006.

C.J. Honey, O. Sporns, L. Cammoun, X. Gigandet, J.P. Thiran, R. Meuli and P. Hagmann. Predicting human resting-state functional connectivity from structural connectivity. *PNAS*, 106: 2035-40, 2009.

Y. Iturria-Medina and E. Canales-Rodriguez. Characterizing brain anatomical connections using diffusion weighted MRI and graph theory. *Neuroimage*, 36: 645-60 2007.

K. J. Friston. Statistical parametric mapping: the analysis of functional brain images. 647, 2007.

M. Koch, D. Norris and M. Hund-Georgiadis. An investigation of functional and anatomical connectivity using magnetic resonance imaging. *Neuroimage*, 16: 241-50, 2002.

P. Kochunov, P. Thompson, J. Lancaster and G. Bartzokis. Relationship between white matter fractional anisotropy and other indices of cerebral health in normal aging: tract-based spatial statistics study of aging. *Neuroimage*, 35: 478-87, 2007.

K. Konrad and S. Eickhoff. Is the ADHD brain wired differently? A review on structural and functional connectivity in attention deficit hyperactivity disorder. *Hum. Brain Mapp.*, 31: 904–16, 2010.

Z. Kou, Z. Wu, K.A. Tong, B. Holshouser, R.R. Benson, J. Hu and E.M. Haacke. The Role of Advanced MR Imaging Findings as Biomarkers of Traumatic Brain Injury. *J Head Trauma Rehab*, 25: 267-82, 2010.

M. Lazar and A. Alexander. Bootstrap white matter tractography (BOOT-TRAC). *Neuroimage*, 2005.

D. Le Bihan, J. Mangin and C. Poupon. Diffusion tensor imaging: concepts and applications. *J. Magn. Reson. Imaging*, 13: 534-46, 2001.

F. Liu, L. Vidarsson, J.D. Winter, H. Tran and A. Kassner. Sex differences in the human corpus callosum microstructure: A combined T-2 myelin-water and diffusion tensor magnetic resonance imaging study. *Brain Res.,* 1343: 37-45, 2010.

B. Mädler, S. Drabycz and S. Kolind. Is diffusion anisotropy an accurate monitor of myelination? Correlation of multicomponent T2 relaxation and diffusion tensor anisotropy in human brain. *Magn. Reson. Imaging,* 26: 874-88, 2008.

R. McKinstry, A. Mathur, J. Miller and A. Ozcan. Radial organization of developing preterm human cerebral cortex revealed by non-invasive water diffusion anisotropy MRI. *Cereb. Cortex,* 12: 1237-43, 2002.

D. Modha and R. Singh. Network architecture of the long-distance pathways in the macaque brain. *PNAS,* 107: 13485–90, 2010.

S. Mori and P. van Zijl. Fiber tracking: principles and strategies-a technical review. *NMR Biomed.,* 15: 468-80, 2002.

R. Müller. The study of autism as a distributed disorder. *Mental retardation and developmental disability research,* 13: 85-95, 2007.

M. O'Sullivan, D. Jones, P. Summers and R. Morris. Evidence for cortical" disconnection" as a mechanism of age-related cognitive decline. *Neurology,* 57: 632-38, 2001.

J. Oh, I. Song, J. Lee, H. Kang, K. Park and E. Kang. Tractography-guided statistics (TGIS) in diffusion tensor imaging for the detection of gender difference of fiber integrity in the midsagittal and parasagittal corpora. *Neuroimage,* 36: 606-16 2007.

G. Parker and H. Haroon. A framework for a streamline-based probabilistic index of connectivity (PICo) using a structural interpretation of MRI diffusion measurements. *J. Magn. Reson. Imaging,* 18: 242–54, 2003.

L. Pollonini, S. Pophale, N. Situ, M.-H. Wu, R.E. Frye, J. Leon-Carrion and G. Zouridakis. Information Communication Networks in Severe Traumatic Brain Injury. *Brain Topogr,* 23: 221-26, 2010.

E. Robinson, M. Valstar and A. Hammers. Multivariate statistical analysis of whole brain structural networks obtained using probabilistic tractography. *MICCAI*: 486-93, 2008.

E.C. Robinson, A. Hammers, A. Ericsson, A.D. Edwards and D. Rueckert. Identifying population differences in whole-brain structural networks: a machine learning approach. *NeuroImage,* 50: 910-19, 2010.

D. Rueckert, L. Sonoda, C. Hayes and D. Hill. Non-rigid registration using free-form deformations: application to breast MR images. *IEEE Trans. Med. Imaging,* 18: 712-21, 1999.

R. Salvador, J. Suckling and M. Coleman. Neurophysiological architecture of functional magnetic resonance images of human brain. *Cereb. Cortex,* 15: 1332-42, 2005.

J. Sled, A. Zijdenbos and A. Evans. A nonparametric method for automatic correction of intensity nonuniformity in MRI data. *IEEE Trans. Med. Imaging,* 17: 87 - 97, 1998.

S. Smith, M. Jenkinson, M. Woolrich, C. Beckmann, T. Behrens, H. Johansen-Berg, P. Bannister, M. De Luca, I. Drobnjak, D. Flitney, R. Niazy, J. Saunders, J. Vickers, Y. Zhang, N. De Stefano, J. Brady and P. Matthews. Advances in functional and

structural MR image analysis and implementation as FSL. *Neuroimage,* 23: 208-19, 2004.

A. Stark and B. Pakkenberg. Histological changes of the dopaminergic nigrostriatal system in aging. *Cell Tissue Res.,* 318: 81-92, 2004.

B.C.M.v. Wijk, C.J. Stam and A. Daffertshofer. Comparing brain networks of different size and connectivity density using graph theory. *PLoS ONE,* 5: e13701, 2010.

A. Zalesky, A. Fornito and E. Bullmore. Network-based statistic: Identifying differences in brain networks. *Neuroimage,* 53: 1197–207, 2010.